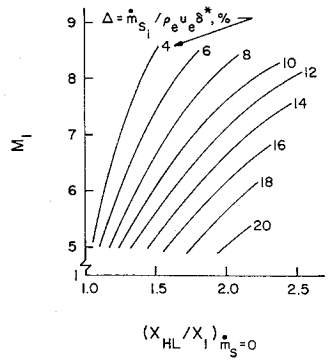

Fig. 4 Generalized mass transfer required to achieve incipient separation for given Mach number and extent of separation.

The mass flow for which $x_{HL} = x_1$ is obtained in Fig. 2 is defined as the incipient condition, $\dot{m}_{si}$. The incipient mass flow is nondimensionalized by the boundary-layer mass defect at $x = x_{HL}$ without separation, i.e., $[\rho_e u_e \delta^*]_{xHL}$, and presented versus the extent of separation without mass removal, i.e., $\dot{m}_s = 0$, in Fig. 3. The utility of the results of Fig. 3 is improved by a cross-plot as shown in Fig. 4 and may be interpreted as follows for the range of conditions investigated. 1) M_1, x_1, x_{HL} and Re_1 are assumed known. 2) For these conditions, the percent of boundary-layer mass defect that is required to be removed by slot suction for incipient separation is obtained by entering Fig. 4 at M_1 and x_{HL}/x_1.

As might be expected for constant M_1, Δ, the nondimensional mass suction, increases as the extent of separation increases. For a constant extent of separation Δ decreases as the Mach number increases.

An analysis for incipient mass flow required for laminar separated boundary layers, similar to that of Ref. 2 and to that of Ref. 3 for turbulent flows, was performed. The first momentum integral equation is integrated assuming constant momentum thickness and a constant transformed form factor at incipient separation, i.e., zero wall shear stress.

The results of such an analysis are shown in Fig. 5 in terms of the inviscid pressure ratio across the hinge line. Considering the simplifying assumptions involved in the analysis, the over-all agreement is much better than expected. The agreement is good for a pressure ratio on the order of 10. For very large mass flows an unrealistic asymptote is obtained for the pressure ratio. The analysis also does not predict a pressure ratio, i.e., a flap deflection angle, that the boundary layer can negotiate without separating.

Conclusions

The effects of slot suction on two-dimensional separated laminar boundary layers have been studied over a Mach number range at the beginning of the interaction of 5.3 to 8 and a Reynolds number per inch range of 0.45×10^5 to 1.45×10^5 at a wall to stagnation temperature ratio of 0.56. For this range of test parameters it is concluded that:

1) The separated laminar boundary layer is very sensitive to slot suction. Removal of a small percentage of the boundary-layer mass defect is sufficient to collapse the separated flow region.

2) By integration of the first momentum integral equation for a compressible laminar boundary layer with the assumption of constant momentum thickness, an expression is obtained for the mass suction required to maintain incipient separation. The results are in fair agreement with experimental results.

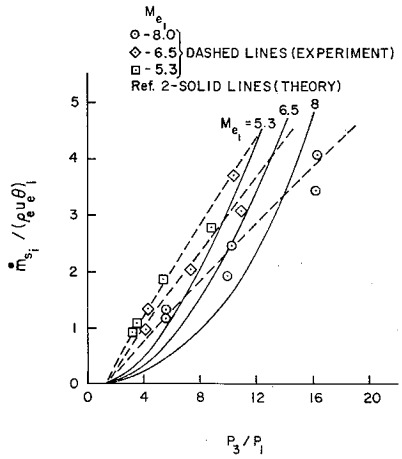

Fig. 5 Comparison of theory with experiment for the mass suction required for incipient separation.

References

[1] Ball, K. O. W. and Korkegi, R. H., "An Investigation of the Effect of Suction on Hypersonic Laminar Boundary-Layer Separation," *AIAA Journal*, Vol. 6, No. 2, Feb. 1968, pp. 239–243.

[2] Ball, K. O. W., "Elimination of Boundary Layer Separation by Slot Suction," *Office of Aerospace Research Review*, Vol. III, No. 2, Feb. 1968.

[3] Pearson, L. W., "Effects of Slot Suction on Turbulent Boundary Layer Separation," AIAA Paper 67–197, New York, 1967.

Electron Density Reduction in Re-Entry Plasma due to Nitrogen Atom Removal

CHARLES J. SCHEXNAYDER*
NASA Langley Research Center, Hampton, Va.

IN the past few years emphasis has been placed on fluid injection methods for reducing electron concentration in the plasma surrounding a re-entry vehicle in order to alleviate the radio blackout. One method, such as the one advanced by Evans of the Langley Research Center, is to use liquid droplets as sites to achieve recombination of electrons and

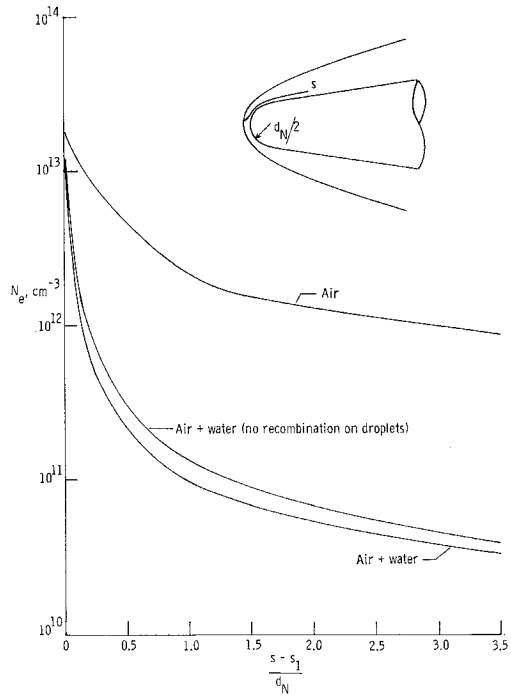

Fig. 1 Reduction in electron concentration due to water injection.

Received August 18, 1969; revision received October 20, 1969.

* Aerospace Engineer, Planetary Gas Kinetics Section, Aero-Physics Division.

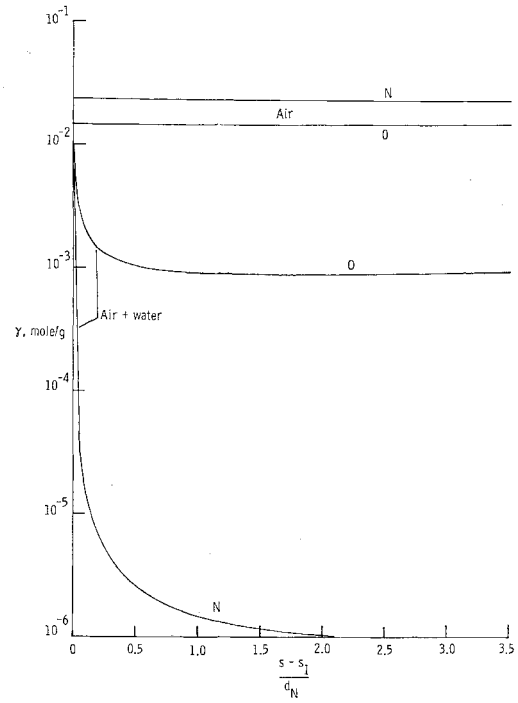

Fig. 2 Streamline variation of nitrogen and oxygen atom concentration.

ions. This method works well in cool, overionized plasmas where the concentration of free electrons is larger than it would be if there were equilibrium at the local gas temperature. In hot plasmas, injection of fluids can be effective in lowering the ionization by simply cooling the plasma. The purpose of this Note is to show that the injection of water droplets into the flow around a vehicle entering the atmosphere at approximately 25,000 fps can result in a reduction of the electron concentration by a method other than the droplet surface recombination or the cooling mechanism.

Figure 1 shows the reduction in electron concentration, N_e, for a typical streamline flowing over a re-entry body at an altitude of 130,000 ft. The curve labeled "air" refers to an inviscid chemical kinetics calculation made using an existing computer program.[1] The electron concentration for this particular streamline is in local ionic equilibrium ($NO^+ + e^- \rightleftarrows N + O$) so that N_e cannot decrease to values lower than those corresponding to equilibrium at the local values of temperature and atom concentrations. Recombination of ions and electrons at the surface of the droplets would have little effect on the over-all N_e since production can be maintained in the plasma. The curves marked "air + water" were calculated using a computer program developed at the NASA Langley Research Center. This program computes the local properties for a one-dimensional streamtube plasma flow of an air-water droplet mixture. The program takes into consideration acceleration and evaporation of the droplets along with a chemical reaction system based on 15 chemical species and 39 homogeneous chemical reactions. The list of species is H_2O, O_2, N_2, H_2, NO, OH, H, O, N, NO^+, N_2^+, N^+, O^+, H^+, and e^-. The specific rate constant for the dissociation of H_2O has the following form:

$$k_i = 3 \times 10^{23} \left(\frac{2.12 \times 10^8 T}{\mu_i}\right)^{1/2} \sigma_i \left(\frac{273.2 D_i}{T} + 1\right)^2 \times \exp\left[-\left(\frac{273.2 D_i}{T} + \frac{3}{2}\right)\right], \frac{\text{cm}^3}{\text{mole-sec}}$$

The specific rate constants for the remaining dissociation reactions have the form

$$k_i = 4.5 \times 10^{23} \left(\frac{2.12 \times 10^8 T}{\mu_i}\right)^{1/2} \times \sigma_i \left(\frac{273.2 D_i}{T} + \frac{1}{2}\right)^{3/2} \exp\left[-\left(\frac{273.2\, D_i}{T} + 1\right)\right], \frac{\text{cm}^3}{\text{mole-sec}}$$

The specific rate constants for reactions 7–39 have the form

$$k_i = 6 \times 10^{23} \left(\frac{2.12 \times 10^8 T}{\mu_i}\right)^{1/2} \sigma_i \times \exp\left[-\left(\frac{273.2 D_i}{T}\right)\right], \frac{\text{cm}^3}{\text{mole-sec}}$$

A list of the reactions used and the constants for the preceding equations are given in Table 1. Five additional heterogeneous reactions account for recombination of electrons and ions at droplet surfaces. These reactions have the following form:

$$k_i = \frac{3u(\hat{})^2 w^* (6.22 \times 10^5 T^{1/2} F_e)}{4 r \rho_l v (1 + f w^*)}, \frac{\text{cm}^3}{\text{g-sec}}$$

where u is gas velocity, v is droplet velocity, r is initial droplet radius, ρ_l is liquid density, $\hat{r}$ is the ratio of droplet radius to

Table 1 Constants for use in reaction rate formulas

i	Reaction	μ_i	D_i	σ_i, cm^2	i	Reaction	μ_i	D_i	σ_i, cm^2
1	$H_2O + M \rightleftarrows OH + H + M$	10.957	217.10	10.00×10^{-16}	21	$N_2 + NO^+ \rightleftarrows N_2^+ + NO$	14.483	268.95	20.00×10^{-16}
2	$O_2 + M \rightleftarrows O + O + M$	14.933	217.34	10.00	22	$N_2 + N^+ \rightleftarrows N_2^+ + N$	9.333	44.19	20.00
3	$N_2 + M \rightleftarrows N + N + M$	14.000	414.50	10.00	23	$N_2 + O^+ \rightleftarrows N_2^+ + O$	10.182	83.70	20.00
4	$H_2 + M \rightleftarrows H + H + M$	1.867	190.34	10.00	24	$N_2 + H^+ \rightleftarrows N_2^+ + H$	0.966	84.12	20.00
5	$NO + M \rightleftarrows N + O + M$	14.483	275.74	10.00	25	$N + NO^+ \rightleftarrows N^+ + NO$	9.545	224.75	20.00
6	$OH + M \rightleftarrows O + H + M$	10.578	186.09	10.00	26	$O + NO^+ \rightleftarrows O^+ + NO$	10.435	185.24	20.00
7	$H + O_2 \rightleftarrows OH + O$	0.970	31.44	1.00	27	$H + NO^+ \rightleftarrows H^+ + NO$	0.968	184.82	20.00
8	$O + H_2 \rightleftarrows OH + H$	1.778	4.25	1.00	28	$N + O^+ \rightleftarrows N^+ + O$	7.467	39.51	20.00
9	$H + NO \rightleftarrows OH + N$	0.968	89.65	1.00	29	$N + H^+ \rightleftarrows N^+ + H$	0.933	39.94	20.00
10	$O + NO \rightleftarrows O_2 + N$	10.435	58.21	1.00	30	$O + H^+ \rightleftarrows O^+ + H$	0.941	0.43	20.00
11	$O + N_2 \rightleftarrows NO + N$	10.182	138.93	2.69	31	$O + NO^+ \rightleftarrows N^+ + O_2$	10.435	282.96	20.00
12	$O + H_2O \rightleftarrows OH + OH$	8.471	31.02	1.00	32	$O + N_2^+ \rightleftarrows N^+ + NO$	10.182	94.74	20.00
13	$H + H_2O \rightleftarrows OH + H_2$	0.947	26.77	1.00	33	$N + NO^+ \rightleftarrows O^+ + N_2$	9.545	46.31	20.00
14	$N + O \rightleftarrows NO^+ + e^-$	7.467	117.69	0.076	34	$N + NO^+ \rightleftarrows N_2^+ + O$	9.545	130.01	20.00
15	$N + N \rightleftarrows N_2^+ + e^-$	7.000	247.27	0.066	35	$H + NO^+ \rightleftarrows N^+ + OH$	0.968	314.40	20.00
16	$N_2 + e^- \rightleftarrows N_2^+ + e^- + e^-$	5.486×10^{-4}	661.94	0.879	36	$NO + O^+ \rightleftarrows N^+ + O_2$	10.435	99.84	20.00
17	$NO^+ + e^- \rightleftarrows NO^+ + e^- + e^-$	5.486×10^{-4}	393.00	0.879	37	$NO + H^+ \rightleftarrows N^+ + OH$	0.968	129.16	20.00
18	$N + e^- \rightleftarrows N^+ + e^- + e^-$	5.486×10^{-4}	617.75	0.879	38	$N_2 + O^+ \rightleftarrows N^+ + NO$	10.182	178.44	20.00
19	$O + e^- \rightleftarrows O^+ + e^- + e^-$	5.486×10^{-4}	578.24	0.879	39	$H_2 + NO^+ \rightleftarrows N^+ + H_2O$	1.875	287.63	20.00
20	$H + e^- \rightleftarrows H^+ + e^- + e^-$	5.486×10^{-4}	577.81	0.879					

initial droplet radius, f is fraction of droplet evaporated, w^* is initial ratio of liquid mass flow to gas mass flow, and F_e is the efficiency factor for capture of electrons by water droplet. For the typical streamtube shown in Fig. 1 water was injected from the side of the vehicle and entered the streamtube at a distance s_1/d_N from the shock with $d_N = 30.48$ cm.

Comparison between these "air + water" curves shows that a large portion of the reduction in N_e, a factor of 10 to 20, is not due to the recombination at the surface of the droplets. Instead, it is due to removal of the condition of local ionic equilibrium which existed before water injection. This is seen in Fig. 2, which shows a decrease in N and O atom concentrations, γ, due to the gas reactions resulting from H_2O dissociation. The rapid removal of the N atom concentration results in a shift away from local equilibrium for the reaction, $NO^+ + e^- \rightleftharpoons N + O$, thus allowing gas phase recombination of $NO^+ + e^-$ to a "self-limiting" level which is based on the local flow velocity and the weakly temperature dependent recombination rate constant.[2] Cooling could not be a factor in shifting from the local equilibrium level to the "self-limiting" level since the temperature of the water + air mixture was actually slightly higher than the temperature of the air without water addition. Calculations of the dilution effect were made and found to be of secondary importance for the amount of water used.

The method presented here for electron density reduction would not be expected to work for blunt-nosed vehicles traveling at velocities much lower than 20,000 fps or much higher than 30,000 fps.

References

[1] Evans, J. S., Schexnayder, C. J., and Huber, P. W., "Ionization in Re-entry Flowfields," *AIAA Journal*, to be published.

[2] Lin, S. C. and Teare, J. D., "A Streamtube Approximation for Calculation of Reaction Rates in the Inviscid Flow Field of Hypersonic Objects," Research Note 223, Aug. 1961, Avco-Everett Research Lab.

Anode Current and Heat Flux Distribution in an MPD Engine

K. T. Shih*
Convair Division of General Dynamics, San Diego, Calif.

Introduction

EXPERIMENTAL results of an anode heat-transfer study of an MPD arc have been previously reported by the author, using a solid anode for the measurement of the total quantities,[1] and a longitudinally segmented anode for the local measurements.[2] Also, a simple anode heat-transfer model was established by which the anode heat flux, Q, may be expressed by

$$Q = I(5kT_e/2e + U_a + \phi) + Q_{cr} \qquad (1)$$

where I is the arc current, k is the Boltzmann constant, e is the electron charge, T_e is the electron temperature outside the anode fall, U_a is the anode fall, ϕ is the work function of the anode material, and Q_{cr} is the anode heat flux due to convection and radiation. Based on this anode heat-transfer model, it was found that the major part of the anode heat flux is carried by the electron current.

Received October 13, 1969. The author gratefully acknowledges stimulating discussions with A. V. Larson and the skillful laboratory work of O. J. Neller. A part of this work was presented as Paper 69-244 at the AIAA 7th Electric Propulsion Conference, Williamsburg, Va., March 3–5, 1969.

* Senior Research Engineer, Sensor Technology. Member AIAA.

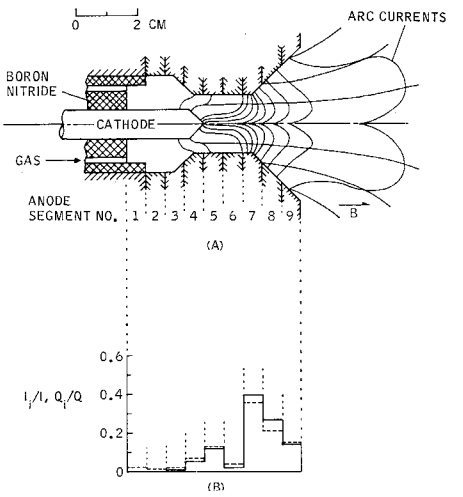

Fig. 1 A: Schematic of MPD arc engine with segmented anode. B: Typical anode current (solid lines) and heat flux (broken lines) distributions, Argon, $\dot{m}$ = 26.5 mg/sec, I = 300 amp, B = 1.6 kgauss, where $I = \Sigma I_i$, $Q = \Sigma Q_i$.

Current distributions have been obtained in the exhaust of an MPD arc by using Hall-effect sensors[3,4] and various search coils.[5] Except for the result of Cann,[3] it was found that only 15% or less of the arc current flows downstream of the anode nozzle. Hence, it is likely that most of the energy and momentum transfer in the arc occurs upstream in the anode nozzle. Due to the experimental difficulty, no current distribution data within the anode nozzle has been measured. In this work, an axially segmented anode is used to measure the axial anode current and heat flux distributions. These distributions provide information about where the important ionization, current, and heat effects take place, and the extent of the high current density zone. They also serve as an independent check of the anode heat-transfer model.

Experimental Apparatus

The engine assembly is shown schematically in Fig. 1a; the anode configuration consists of nine segments cut perpendicularly to the electrode center line. Each segment is isolated both electrically and thermally from the neighboring segments. All segments are water-cooled and connected to a common base ring through individual shunts. The segmented heat fluxes are measured by calorimetric methods, and the segmental currents are obtained by the voltage drop across the shunts. Experiments are conducted in a vacuum tank with a background pressure of less than one micron. Reference 6 presents a detailed description of the test facility.

Experimental Results

Anode current and heat flux distributions have been obtained for the MPD engine in argon by using a segmented anode over a current range from 100 to 500 amp; at mass flow rates from 10 to 40 mg/sec and applied magnetic field strength (measured at the cathode tip) from 0.3 to 3 kgauss. This range of parameters covers both spoke and no-spoke mode.[6,8]

Figure 1b shows typical distribution curves of anode current and heat flux. In this figure, the solid and broken lines represent the current and heat flux distribution, respectively. Generally speaking, the anode current attachment is quite diffuse; it is certainly less constrictive than that predicted by Refs. 5 and 7. The distribution assumes a maximum of about 45 to 50% of the total current to one segment at the